Heliyon 10 (2024) e37134

Contents lists available at ScienceDirect

Heliyon

journal homepage: www.cell.com/heliyon

Research article

Simultaneous removal and separate recovery of radioactive Cs^+ and I^- ions from wastewater using a reusable bifunctional composite, $Ni@Pt/K_2NiFe(CN)_6$

Hwakyeung Jeong [a], Dong Woo Lee [a], Jihye Kim [a], Sang-Eun Bae [a,b,*]

[a] Nuclear Chemistry Technology Division, Korea Atomic Energy Research Institute, 989-111 Daedeok- daero, Yuseong-gu, Daejeon 34057, Republic of Korea

[b] Department of Nuclear Science and Technology, University of Science and Technology, 217 Gajeong-ro Yuseong-gu, Daejeon 34113, Republic of Korea

ARTICLE INFO

Keywords:
Bifunctional composite
Cesium and iodine removal
Separate recovery
Reusable
Electrochemical control

ABSTRACT

Radioactive Cs^+ and I^- ions are major components of nuclear wastewater, typically existing as counter ions. Due to their high water solubility and mobility, these ions can spread through contaminated water and soil into ecosystems, necessitating continuous removal and management. In this study, we synthesized a reusable bifunctional $Ni@Pt/K_2NiFe(CN)_6$ composite that can simultaneously remove radioactive Cs^+ and I^- ions and, for the first time, enable their separate recovery in aqueous solutions. In this material, $K_2NiFe(CN)_6$ acted as an electrochemically switched ion exchanger, controlling the adsorption/desorption of Cs^+, while Pt enabled the spontaneous adsorption and electrochemical desorption of I^-, and the magnetic Ni core allowed for efficient adsorbent recovery. The adsorption isotherms of both Cs^+ and I^- were best fitted using the Langmuir model, and the corresponding adsorption capacities were comparable to those of conventional adsorbents used for the separate removal of Cs^+ and I^-. Furthermore, the composite demonstrated stability over 100 sorption cycles, maintaining high recovery efficiencies of 97.9 % for Cs^+ and 99.7 % for I^-, thereby proving its reusability. Thus, the developed composite holds great promise for radioactive wastewater treatment and environmental restoration.

Environmental Implication

Radioactive Cs^+ and I^- ions are the major components of nuclear wastewater. Due to high water-solubility and mobility, they can easily enter the human through the food chain, posing serious health problems. In this study, we synthesized a reusable bifunctional composite, $Ni@Pt/K_2NiFe(CN)_6$, capable of simultaneously removing radioactive Cs^+ and I^- from aqueous solutions and allowing for their separate recovery. Within the composite, $K_2NiFe(CN)_6$ is responsible for Cs^+ adsorption, while the Pt is responsible for I^- adsorption. The adsorbent demonstrates stability over 100 cycles of Cs^+ and I^- removal and recovery, underscoring its promising potential for nuclear waste management.

* Corresponding author. Nuclear Chemistry Technology Division, Korea Atomic Energy Research Institute, 989-111 Daedeok- daero, Yuseong-gu, Daejeon 34057, Republic of Korea.

E-mail address: sebae@kaeri.re.kr (S.-E. Bae).

https://doi.org/10.1016/j.heliyon.2024.e37134
Received 9 July 2024; Received in revised form 21 August 2024; Accepted 28 August 2024
Available online 29 August 2024

1. Introduction

Nuclear power plants remain one of the most important sources of electrical energy due to their high price competitiveness, low carbon dioxide emissions, and partially reusable fuels [1,2]. However, the efficient managing the radioactive wastewater discharged from these plants and the safely disposing of radioactive species released during nuclear accidents remain a significant global challenge [3–6]. Additionally, the safe treatment of radioactive wastewater generated from medical nuclear applications and various extractive industries is also crucial [7]. Among the various radioisotopes, Cs^+ and I^- ions are the major components of radioactive wastewater [8]. These ions exhibit high water solubility and mobility, causing serious health problems upon entering the human through the food chain [9–11]. Therefore, the removal of these radioactive species from wastewater has garnered considerable attention.

Among the materials used to remove radioactive cesium, such as inorganic ion exchangers and clay minerals [12–14], electroactive ion exchangers like hexacyanoferrates have a particular advantage. These materials can selectively adsorb and desorb Cs^+ through an electrochemically switched ion-exchange process, making them reusable [15–17]. Similarly, the removal of iodine from wastewater is commonly accomplished using zeolites, metal-organic frameworks, and composites [18–21]. Recently, a reusable adsorbent based on Pt-coated magnetic metal nanoparticles has been developed to remove iodine from aqueous solutions and electrochemically separate the adsorbed iodine [22].

To date, most of the relevant study has been focused on the removal of Cs^+ and I^-, primarily on the development of adsorbents with maximum adsorption capacity and direct disposal of the adsorbents after use. Some studies have reported adsorbents that can simultaneously capture cesium and iodine [23–25], which typically coexist as counter ions in liquid waste. However, directly disposing of the cesium (^{137}Cs, $t_{1/2} = 30.1$ years) and iodine (^{129}I; $t_{1/2} = 15.7 \times 10^7$ years) together can pose challenges for managing radioactive waste storage due to their significantly different nuclear decay half-lives.

Herein, we developed a reusable bifunctional composite ($Ni@Pt/K_2NiFe(CN)_6$) for the simultaneous adsorptive removal and separate release of radioactive Cs^+ and I^-. The magnetic Ni core accounted for efficient adsorbent recovery, while $K_2NiFe(CN)_6$ and Pt were responsible for the adsorption/desorption of Cs^+ and I^-, respectively. This innovative approach uses electrochemical separation processes to simultaneously capture Cs^+ and I^- species and then separately release them in the next step, significantly reducing the volume of radioactive waste. The prepared composite exhibited performance comparable to state-of-the-art adsorbents used for the separate removal of Cs^+ and I^-, demonstrating great promise for the disposal of wastewater contaminated with radioactive cesium and iodine.

2. Material and methods

2.1. Chemicals

Ni nanoparticle (>99.5 %, average particle size = 40 nm) was obtained from US Research Nanomaterials (USA). K_2PtCl_6 and CsI (99.999 %) were obtained from Alfa Aesar Co. Others, including $K_4Fe(CN)_6$ (≥98.51 %), $CsNO_3$ (99 %), and $NaClO_4$ (≥98 %) were obtained from Sigma-Aldrich Co. HNO_3 and ethanol were obtained from Merck Millipore. All solutions were prepared using purified water (Milli-Q, 18.2 MΩ cm).

2.2. Preparation of $Ni@Pt/K_2NiFe(CN)_6$

$Ni@Pt/K_2NiFe(CN)_6$ was synthesized by coating magnetic Ni nanoparticles with Pt and $K_2NiFe(CN)_6$ (Fig. 1(a)). K_2PtCl_6 (1.0 g) was added to 0.2 M HNO_3 (100 mL) containing Ni nanoparticles (0.75 g), and the resulting mixture was vigorously shaken for 10 min. As a result, Pt was spontaneously coated on the Ni core surface due to the difference in the related standard reduction potentials [26]. The solution was then supplemented with $K_4Fe(CN)_6$ (1.0 g) and allowed to react for 12 h, leading to the formation of $K_2NiFe(CN)_6$ via the spontaneous substitution reaction between the K^+ ions of $K_4Fe(CN)_6$ and the Ni core metal [27]. The prepared $Ni@Pt/K_2NiFe(CN)_6$ could be easily recovered using a Nd magnet (Fig. 1(b)). Ni@Pt and $Ni@K_2NiFe(CN)_6$ were prepared in the same manner but without the addition of $K_4Fe(CN)_6$ and K_2PtCl_6, respectively. The composites were washed several times with ethanol and distilled water before use.

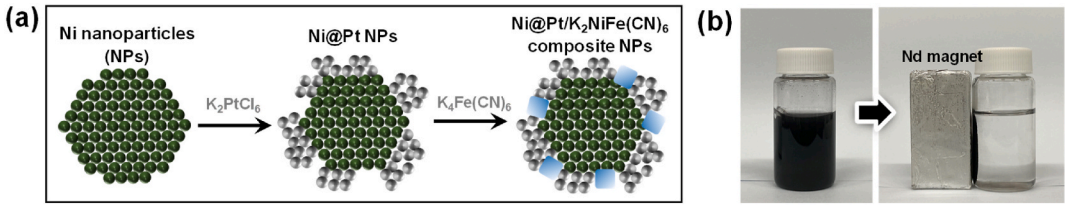

Fig. 1. (a) Schematic of the synthesis of $Ni@Pt/K_2NiFe(CN)_6$ (cross-sectional structure) and (b) photograph demonstrating its magnetic separation.

2.3. Characterization and instrumentation

The morphology and composition of Ni@Pt/$K_2NiFe(CN)_6$ were investigated using transmission electron microscopy (TEM) coupled with energy-dispersive X-ray spectroscopy (EDS) on a JEOL JEM-2100F microscope (JEOL Ltd, Japan) operated at an accelerating voltage of 200 kV. Phase composition and crystallinity were examined by powder X-ray diffraction (XRD) measurements, performed on a Bruker D8 Advance diffractometer (Bruker, Germany) using Cu K_α radiation at 40 kV and 40 mA. The polycrystalline samples were scanned in the 2θ range from 20° to 60° with a step size (0.02°) and a step time (0.1 s). The oxidation state of elements constituting Ni@Pt/$K_2NiFe(CN)_6$ was examined using X-ray absorption spectroscopy (XAS) measurements at the 2A beamline of the Pohang Light Source. The total electron yield method was used, and the drain current of the gold mesh was measured simultaneously with that of samples to normalize beam current.

All electrochemical measurements were conducted using a CHI 660D workstation (CH Instruments, USA). The working electrode was a glassy carbon (GC) rod (0.071 cm^2) or plate (9 cm^2), while the reference and counter electrodes corresponded to Ag|AgCl (3 M NaCl) and a graphite rod, respectively. For cyclic voltammetry measurement, an aqueous dispersion of the sample was covered on a glass carbon rod or plate. Prior to electrochemical measurements, a Nafion solution (0.05 wt%) was dropped onto the electrode.

Cs^+ and I^- concentrations were quantified using inductively coupled plasma-mass spectrometry (iCAP-Qc, Thermo Fisher Scientific, USA) and UV–vis absorption spectroscopy (Biochrom WPA Lightwave II, Biochrom Ltd, USA), respectively.

2.4. Adsorption experiments

Adsorption experiments were performed at room temperature (~25 °C). The time-dependent efficiency of Cs^+ and I^- adsorption on Ni@Pt/$K_2NiFe(CN)_6$ was probed by adding 100 mg of the composite to 50 mg/L CsI (10 mL) in 0.1 M $NaClO_4$ and quantifying Cs^+ and I^- after certain exposure times. The time required to establish adsorption equilibrium for both Cs^+ and I^- was determined to be 10 h (Fig. S1). In a series of experiments to obtain adsorption isotherms, variable-concentration solutions of CsI (10 mL) in 0.1 M $NaClO_4$ (pH 7) were supplemented with 30 mg of Ni@Pt/$K_2NiFe(CN)_6$ and allowed to react for 12 h to provide sufficient adsorption time. The

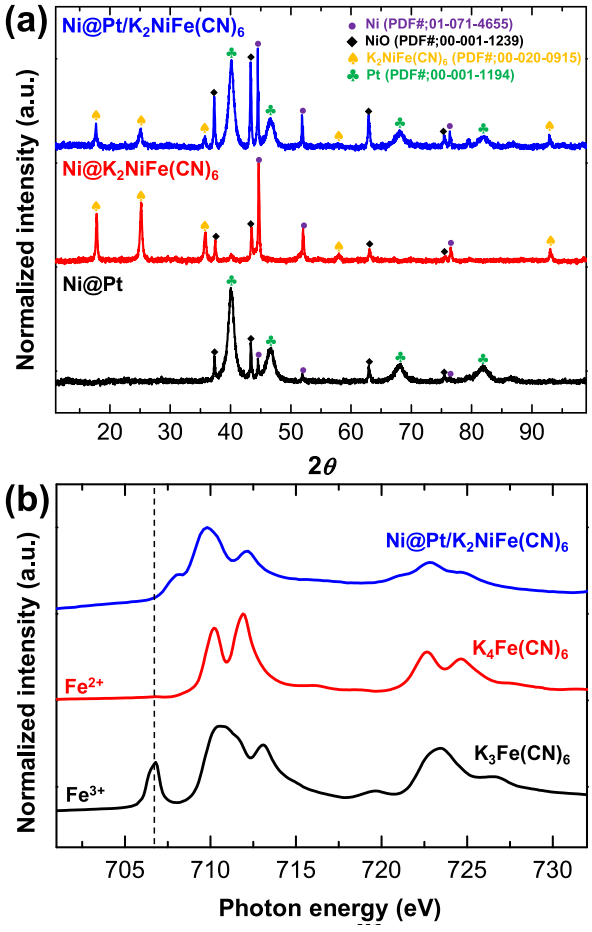

Fig. 2. (a) XRD patterns of Ni@Pt, Ni@$K_2NiFe(CN)_6$, and Ni@Pt/$K_2NiFe(CN)_6$, and (b) Fe L-edge XAS spectra of Ni@Pt/$K_2NiFe(CN)_6$, $K_3Fe(CN)_6$, and $K_4Fe(CN)_6$.

equilibrium adsorption capacities for Cs^+ and I^- (q_e, mg/g) were determined as

$$q_e = \frac{(C_i - C_e) \times V}{M},$$

where C_i and C_e (mg/L) are the initial and equilibrium concentrations of Cs^+ and I^- in the solution, respectively, V (L) is the solution volume, and M (g) is the adsorbent mass.

2.5. Electrochemical separation

The electrochemical separation of Cs^+ and I^- was achieved using chronoamperometry. During the adsorption, a constant potential of 0.0 V (1 step) was applied for 1000 s to a Ni@Pt/$K_2NiFe(CN)_6$-loaded GC electrode in a 10 mg/L CsI-containing solution. The electrode was then washed with distilled water and transferred to a solution without CsI. Desorption of I^- and Cs^+ was performed by sequentially applying potentials of −0.9 V (2 step, I^- desorption) [22] and 0.8 V (3 step, Cs^+ desorption) [28] for 1000 s each. If Cs^+ is desorbed first, I^- adsorbed on the Pt surface can be oxidized to I_2 simultaneously. Therefore, to treat them efficiently, I^- was desorbed first. The electrochemical separation cycle, which involves adsorption and desorption, was repeated several times. Small aliquots of the solution were collected at each cycle, and the concentrations of Cs^+ and I^- in the solution were determined by ICP-MS analysis.

3. Results and discussion

3.1. Characterization of Ni@Pt/$K_2NiFe(CN)_6$

Fig. 2(a) displayed the XRD patterns of Ni@Pt/$K_2NiFe(CN)_6$, Ni@Pt, and Ni@$K_2NiFe(CN)_6$, all showing peaks corresponding to Ni and NiO derived from the Ni core. The Ni@Pt and Ni@$K_2NiFe(CN)_6$ patterns exhibited characteristic peaks for Pt and $K_2NiFe(CN)_6$, respectively, while the Ni@Pt/$K_2NiFe(CN)_6$ pattern displayed peaks for both Pt and $K_2NiFe(CN)_6$. Fig. 2(b) presented the Fe L2,3-edge XAS spectra of Ni@Pt/$K_2NiFe(CN)_6$, $K_3Fe(CN)_6$, and $K_4Fe(CN)_6$. The absence of the Fe^{3+} peak at ~707 eV [29] in the spectrum of Ni@Pt/$K_2NiFe(CN)_6$ suggested that Fe in $K_2NiFe(CN)_6$ exists as Fe^{2+}.

Fig. 3(a) presented a representative TEM image of Ni@Pt/$K_2NiFe(CN)_6$, showing Ni core nanoparticles with a roughened surface due to the deposited Pt and $K_2NiFe(CN)_6$ particles. Although the particles were challenging to distinguish based on their morphology using TEM alone, EDS mapping results (Fig. 3(b–d)) indicated the homogeneous distribution of both Pt and Fe on the Ni core. These results aligned with the XRD analysis, suggesting the coexistence of Pt and $K_2NiFe(CN)_6$ on the Ni core surface.

3.2. Electrochemical properties

The $K_2NiFe(CN)_6$ exchanger possesses an open framework with a face-centered cubic structure, where Fe and Ni ions occupy the corners of the elementary cubes, cyano groups line the edges, and exchangeable K^+ ions reside at the body center. Hydrated alkali-metal ions such as Cs^+ can penetrate into the structure [30].

To investigate the electrochemically switched ion-exchange properties of $K_2NiFe(CN)_6$ for alkali-metal cations, cyclic voltammograms of Ni@Pt/$K_2NiFe(CN)_6$ were recorded in $NaClO_4$. The redox peak observed at ~0.3 V vs. Ag/AgCl (Fig. 4) was due to the change in the oxidation state of Fe in $K_2NiFe(CN)_6$ accompanied by the intercalation/deintercalation of alkali-metal ions, as shown in the equation below [28,31].

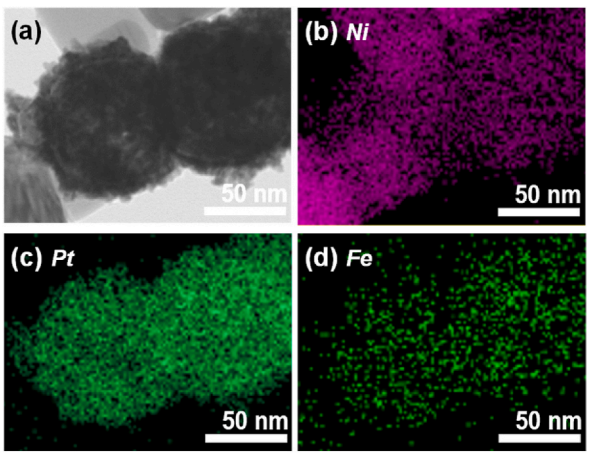

Fig. 3. (a) Representative TEM image of Ni@Pt/$K_2NiFe(CN)_6$, and (b–d) related EDS mapping images showing the distributions of (b) Ni, (c) Pt, and (d) Fe.

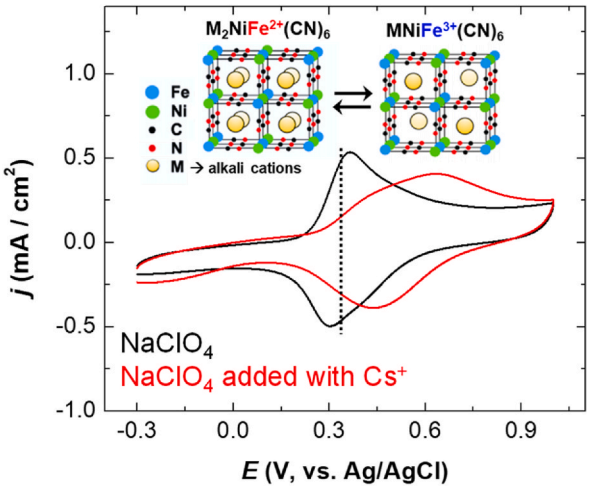

Fig. 4. Cyclic voltammograms of a Ni@Pt/$K_2NiFe(CN)_6$-loaded (0.3 mg/cm^2) GC-rod electrode recorded in 0.1 M $NaClO_4$ (pH 7) in the presence and absence of 10 mM $CsNO_3$ (scan rate = 50 mV/s).

$M_2Ni[Fe^{II}(CN)_6] \leftrightarrow MNi[Fe^{III}(CN)_6] + M^+ + e^-$ (M = alkali metal)

Upon the introduction of Cs^+ into the electrolyte, the peak shifted to higher values, as has been observed for conventional metal hexacyanoferrates [32]. This shift was ascribed to the dependence of the redox peak potential on the hydrated radius of the alkali-metal cation; in particular, the intercalation of Cs^+ is thermodynamically more favorable than those of other alkali-metal cations [33]. Moreover, no shift was observed upon the addition of Cs^+ when the electrode was loaded with Ni@Pt only (Fig. S2). These results indicated that the presence of $K_2NiFe(CN)_6$ on the composite surface and the electrochemical control of the Fe oxidation state enabled the intercalation/deintercalation of Cs^+. In the electrochemical separation process, potentials of 0.0 and 0.8 V were applied to achieve the adsorption and desorption of Cs^+, respectively.

I^- is spontaneously chemisorbed on Pt surfaces from aqueous solution, involving hydrogen evolution and the formation of a covalent bond between Pt and I: [22,34].

$Pt\ (111) + I^- + H_2O \rightarrow Pt\text{-}I(ads) + OH^- + 0.5H_2$.

The adsorptions of the iodide ion on the Pt surface were interrogated using UV–vis absorption spectroscopy (Fig. 5 inset). The absorption band of the iodide ion at 226 nm disappeared upon the addition of Ni@Pt/$K_2NiFe(CN)_6$ to the CsI solution, indicating the removal of I^- via spontaneous adsorption on Pt. Subsequently, the electrochemical behavior of iodine adsorbed on the Pt surface of

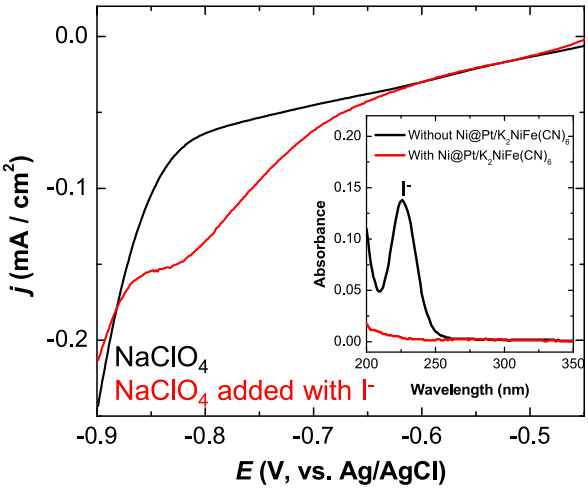

Fig. 5. Cyclic voltammograms of a Ni@Pt/$K_2NiFe(CN)_6$-loaded (0.3 mg/cm^2) GC-rod electrode recorded in 0.1 M $NaClO_4$ (pH 7) in the presence and absence of 10 mM CsI (scan rate = 50 mV/s). The inset shows the UV–vis absorption spectra of the 0.1 mM CsI +0.1 M $NaClO_4$ (pH 7) solution recorded before and after the removal of I^- with Ni@Pt/$K_2NiFe(CN)_6$.

Ni@Pt/$K_2NiFe(CN)_6$ was investigated using cyclic voltammetry. The reduction peak observed between −0.6 and −0.9 V in Fig. 5 was attributed to the desorption of iodine; therefore, a potential, −0.9 V, was applied to separate the Pt-bound iodine in the electrochemical separation process.

3.3. Adsorption isotherm experiments

Prior to performing electrochemical separation, we evaluated the adsorption capacities of Ni@Pt/$K_2NiFe(CN)_6$ for Cs^+ and I^-. Adsorption isotherms were obtained by analyzing Cs^+ and I^- concentrations before and after exposing variable-concentration CsI solutions to Ni@Pt/$K_2NiFe(CN)_6$ for 12 h at room temperature. The classic Langmuir model was used to describe the adsorption equilibrium (Fig. 6) [35,36].

$$\frac{C_e}{q_e} = \frac{1}{k\, q_m} + \frac{C_e}{q_m},$$

where q_m (mg/g) represents the theoretical maximum adsorption capacity corresponding to complete monolayer coverage, and k is the adsorption constant of the Langmuir model. The inset of Fig. 6 demonstrated that the Langmuir isotherms for both Cs^+ and I^- could be well fitted by a straight line across the entire concentration range, indicative of monolayer adsorption on a homogeneous surface [37]. Additionally, the Freundlich model was utilized to characterize adsorption behavior (Fig. S3); however, the corresponding correlation factors (R^2) were lower than those of the Langmuir model.

$$\log q_e = \frac{1}{n}\log c_e + \log k_F,$$

where k_F is the Freundlich isotherm constant and n is the exponential constant related to the adsorption intensity [38].

The maximum adsorption capacity for I^- exceeded that for Cs^+ due to the higher amount of Pt present on the Ni surface compared to $K_2NiFe(CN)_6$ (Fig. 2c and d)). To verify that I^- was not adsorbed on $K_2NiFe(CN)_6$, we added $K_2NiFe(CN)_6$ nanoparticles into a solution containing I^-, waited to establish an equilibrium, and then performed cyclic voltammetry measurements (Fig. S4). No current peak related to the desorption of I^- on $K_2NiFe(CN)_6$ was observed.

3.4. Electrochemical separation

To evaluate the performance of Ni@Pt/$K_2NiFe(CN)_6$ for the simultaneous and repeated removal of Cs^+ and I^- from aqueous solutions, electrochemical separation was conducted. In this process, the adsorption and desorption of Cs^+ and I^- were controlled by applying potential under magnetic stirring. Fig. 7(a) illustrated the removal and recovery process of Cs^+ and I^- dissolved in an aqueous solution using Ni@Pt/$K_2NiFe(CN)_6$ as a reusable adsorbent.

Ni@Pt/$K_2NiFe(CN)_6$ was added to an aqueous solution containing CsI (1 step); applying an adsorption potential, 0.0 V, results in the simultaneously adsorption of Cs^+ and I^-. The adsorbent was moved to a new electrolyte solution where the iodine adsorbed on the adsorbent was desorbed by applying a potential of −0.9 V (2 step). And then the adsorbent was moved to second new electrolyte solution to desorb the Cs^+ ions by applying +0.8 V (3 step). Here the sequence of the desorbing was crucial. If the Cs desorption was performed first, the iodine could be desorbed along with it due to its oxidation at the potential of +0.8 V. This process allowed for the simultaneous separation of Cs^+ and I^- from the aqueous waste solution, followed by their release into two separate aqueous solutions. This method enabled the simultaneous recovery and separate disposal of Cs^+ and I^- ions according to the disposal policies for each

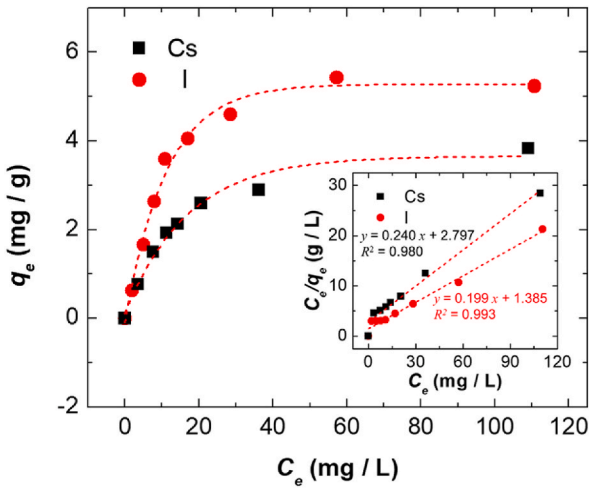

Fig. 6. Isotherms for Cs^+ and I^- adsorption on Ni@Pt/$K_2NiFe(CN)_6$. The inset shows the corresponding C_e/q_e vs. C_e plots and the related linear fits.

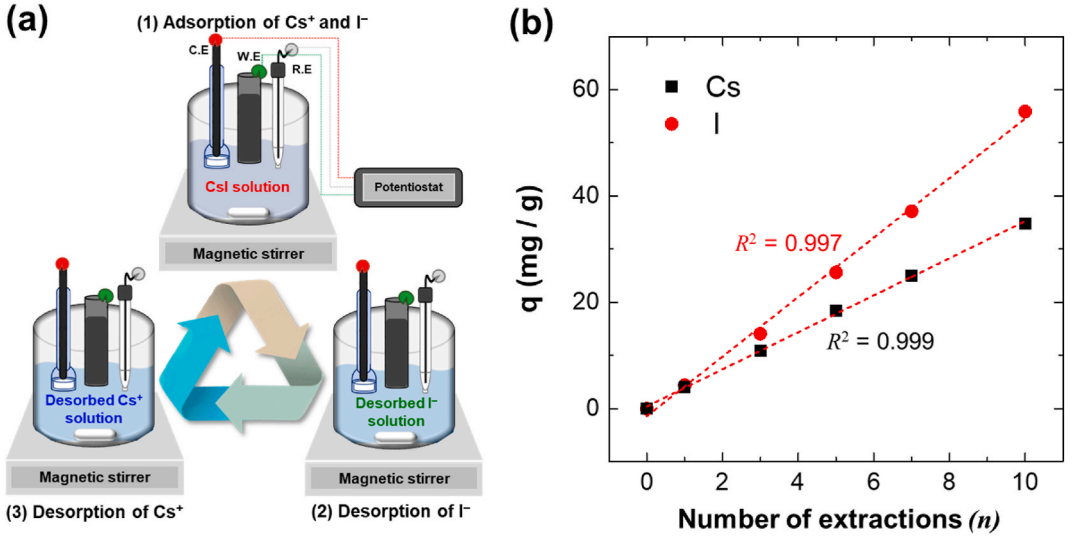

Fig. 7. (a) Schematic of electrochemical separation of Cs^+ and I^- using a Ni@Pt/$K_2NiFe(CN)_6$-loaded (4.4 mg/cm^2) GC-plate electrode, and (b) variation of Cs^+ and I^- concentrations with the number of electrochemical separation steps.

element.

Upon repetitive electrochemical separation, Cs^+ and I^- were continuously adsorbed and desorbed, and the concentrations of these two ions linearly increased with the number of cycles (Fig. 7(b)). After 10 consecutive adsorption/desorption cycles, the Cs^+ and I^- adsorption capacities were measured at 35 mg/g and 56 mg/g, respectively, which are comparable to those of other adsorbents (see Table S1). The adsorption capacity under electrochemical control was confirmed to be at a similar level to the maximum adsorption capacities measured from the spontaneous adsorption reaction.

To test the stability of Ni@Pt/$K_2NiFe(CN)_6$ adsorbents over repetitive applications for the adsorptive removals and recoveries of Cs^+ and I^- ions, we conducted sorption experiments for 100 cycles. Fig. 8 showed XAS spectra of the adsorbents recorded before the separation and after 50 and 100 separation cycles. Clear X-ray absorption spectrum for the Ni core covered by Pt and $K_2NiFe(CN)_6$ layers confirmed that the core Ni nanoparticles are intact and stable without dissolution during the cesium and iodine species removal and recovery processes. For the stability test, cyclic voltammograms of Ni@Pt/$K_2NiFe(CN)_6$ were also recorded in 0.1 M $NaClO_4$ (pH 7) containing (a) 10 mM $CsNO_3$ and (b) 10 mM CsI before and after 100 separation cycles (Fig. S5). After reusing the Ni@Pt/$K_2NiFe(CN)_6$ adsorbent 100 times, the recovery efficiencies of Cs^+ and I^- were determined to be 97.9 % and 99.7 %, respectively. Thus, the prepared Ni@Pt/$K_2NiFe(CN)_6$ adsorbents in this work kept high recovery efficiencies for cesium and iodine removal and demonstrated substantial recyclability over 100 cycles.

4. Conclusion

In this work, we developed a reusable bifunctional composite Ni@Pt/$K_2NiFe(CN)_6$, which effectively removes and separately recovers radioactive Cs^+ and I^- ions from wastewater. In this composite, $K_2NiFe(CN)_6$ is responsible for Cs^+ adsorption, while Pt handles I^- adsorption. The composite's performance is comparable to conventional adsorbents for the separate removal of Cs^+ and I^-, with maximum adsorption capacities of 35 mg/g for Cs^+ and 56 mg/g for I^-. It demonstrated stability over 100 sorption cycles, maintaining high recovery efficiencies of 97.9 % for Cs^+ and 99.7 % for I^-. Overall, the developed Ni@Pt/$K_2NiFe(CN)_6$ composite shows promise for managing radioactive wastewater contaminated with Cs^+ and I^- ions, offering a strategic approach for treating and disposing of these ions separately according to the disposal policies.

CRediT authorship contribution statement

Hwakyeung Jeong: Writing – original draft, Visualization, Methodology, Investigation, Formal analysis, Data curation. **Dong Woo Lee:** Methodology. **Jihye Kim:** Investigation. **Sang-Eun Bae:** Writing – review & editing, Supervision, Resources, Project administration, Methodology, Funding acquisition, Data curation, Conceptualization.

Declaration of competing interest

The authors declare the following financial interests/personal relationships which may be considered as potential competing interests: Sang-Eun Bae reports financial support was provided by National Research Foundation of Korea. If there are other authors, they declare that they have no known competing financial interests or personal relationships that could have appeared to influence the work

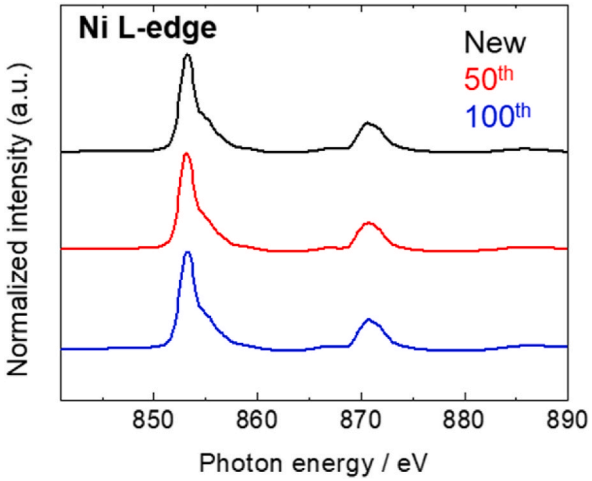

Fig. 8. Ni L-edge XAS spectra of Ni@Pt/$K_2NiFe(CN)_6$ recorded after 0, 50, and 100 separation cycles.

reported in this paper.

Acknowledgments

This work was supported by the National Research Foundation of Korea (NRF), funded by the Ministry of Science and ICT (NRF-2017M2A8A5014716, 2021M2E1A1085202, and RS-2023-00261146) and by Korea Institute of Energy Technology Evaluation and Planning (KETEP) grant funded by the Ministry of Trade Industry and Energy (MOTIE) (RS-2023-0233621).

Appendix A. Supplementary data

Supplementary data to this article can be found online at https://doi.org/10.1016/j.heliyon.2024.e37134.

References

[1] S. Hong, C.J.A. Bradshaw, B.W. Brook, Global zero-carbon energy pathways using viable mixes of nuclear and renewables, Appl. Energy 143 (2015) 451–459.
[2] M.M. Mekonnen, P.W. Gerbens-Leenes, A.Y. Hoekstra, The consumptive water footprint of electricity and heat: a global assessment, Environ. Sci.: Water Res. Technol. 1 (2015) 285–297.
[3] J.E. Ten Hoeve, M.Z. Jacobson, Worldwide health effects of the Fukushima Daiichi nuclear accident, Energy Environ. Sci. 5 (2012) 8743–8757.
[4] X. Liu, J. Wu, L.-a. Hou, J. Wang, Fouling and cleaning protocols for forward osmosis membrane used for radioactive wastewater treatment, Nucl. Eng. Technol. 52 (2020) 581–588.
[5] D. Deng, L. Zhang, M. Dong, R.E. Samuel, A. Ofori-Boadu, M. Lamssali, Radioactive waste: a review, Water Environ. Res. 92 (2020) 1818–1825.
[6] L.A. Poggi, A. Malizia, J.F. Ciparisse, P. Gaudio, A novel integrated approach for the hazardous radioactive dust source terms estimation in future nuclear fusion power plants, Heliyon 2 (2016) 13837.
[7] W.A. Muslim, T.M. Albayati, S.K. Al-Nasri, Decontamination of actual radioactive wastewater containing 137Cs using bentonite as a natural adsorbent: equilibrium, kinetics, and thermodynamic studies, Sci. Rep. 12 (2022) 13837.
[8] Y.H. Ismail, K. Wang, M. Al Shehhi, A. Al Hammadi, Iodide ion-imprinted chitosan beads for highly selective adsorption for nuclear wastewater treatment applications, Heliyon 10 (2024) 13837.
[9] R. Ikehara, K. Morooka, M. Suetake, T. Komiya, E. Kurihara, M. Takehara, R. Takami, C. Kino, K. Horie, M. Takehara, S. Yamasaki, T. Ohnuki, G.T.W. Law, W. Bower, B. Grambow, R.C. Ewing, S. Utsunomiya, Abundance and distribution of radioactive cesium-rich microparticles released from the Fukushima Daiichi Nuclear Power Plant into the environment, Chemosphere 241 (2020) 125019.
[10] S. Sarina, A. Bo, D. Liu, H. Liu, D. Yang, C. Zhou, N. Maes, S. Komarneni, H. Zhu, Separate or simultaneous removal of radioactive cations and anions from water by layered sodium vanadate-based sorbents, Chem. Mater. 26 (2014) 4788–4795.
[11] K. Umadevi, D. Mandal, Performance of radio-iodine discharge control methods of nuclear reprocessing plants, J. Environ. Radioact. 234 (2021) 106623.
[12] J. Wang, S. Zhuang, Cesium separation from radioactive waste by extraction and adsorption based on crown ethers and calixarenes, Nucl. Eng. Technol. 52 (2020) 328–336.
[13] X. Liu, G.-R. Chen, D.-J. Lee, T. Kawamoto, H. Tanaka, M.-L. Chen, Y.-K. Luo, Adsorption removal of cesium from drinking waters: a mini review on use of biosorbents and other adsorbents, Bioresour. Technol. 160 (2014) 142–149.
[14] H. Deng, Y. Li, Y. Huang, X. Ma, L. Wu, T. Cheng, An efficient composite ion exchanger of silica matrix impregnated with ammonium molybdophosphate for cesium uptake from aqueous solution, Chem. Eng. J. 286 (2016) 25–35.
[15] R. Chen, M. Asai, C. Fukushima, M. Ishizaki, M. Kurihara, M. Arisaka, T. Nankawa, M. Watanabe, T. Kawamoto, H. Tanaka, Column study on electrochemical separation of cesium ions from wastewater using copper hexacyanoferrate film, J. Radioanal. Nucl. Chem. 303 (2015) 1491–1495.
[16] J.-Y. Su, G.-P. Jin, T. Chen, X.-D. Liu, C.-N. Chen, J.-J. Tian, The characterization and application of prussian blue at graphene coated carbon fibers in a separated adsorption and electrically switched ion exchange desorption processes of cesium, Electrochim. Acta 230 (2017) 399–406.
[17] Z. Wang, S. Guo, Z. Wu, H. Fan, G. Guan, X. Hao, A smart potential-responsive ion exchange nanomaterial with superparamagnetism for cesium ion separation and recovery, Sep. Purif. Technol. 187 (2017) 199–206.

[18] F. Yu, Y. Chen, Y. Wang, C. Liu, W. Ma, Enhanced removal of iodide from aqueous solution by ozonation and subsequent adsorption on Ag-Ag2O modified on Carbon Spheres, Appl. Sur. Science 427 (2018) 753–762.
[19] P. Mao, Y. Liu, X. Liu, Y. Wang, J. Liang, Q. Zhou, Y. Dai, Y. Jiao, S. Chen, Y. Yang, Bimetallic AgCu/Cu2O hybrid for the synergetic adsorption of iodide from solution, Chemosphere 180 (2017) 317–325.
[20] P. Wang, Q. Xu, Z. Li, W. Jiang, Q. Jiang, D. Jiang, Exceptional iodine capture in 2D covalent organic frameworks, Adv. Mater. 30 (2018) 1801991.
[21] D.K. Harijan, V. Chandra, T. Yoon, K.S. Kim, Radioactive iodine capture and storage from water using magnetite nanoparticles encapsulated in polypyrrole, J. Hazard Mater. 344 (2018) 576–584.
[22] H. Jeong, D.W. Lee, S.J. Hong, J. Kim, M. Kim, J. Kim, H.S. Lee, T.-H. Park, H.-K. Kim, J.I. Park, J.-Y. Kim, S.H. Lim, T. Hyeon, B. Han, S.-E. Bae, Selective removal of radioactive iodine from water using reusable Fe@Pt adsorbents, Water Res. 222 (2022) 118864.
[23] K.-C. Song, H.K. Lee, H. Moon, K.J. Lee, Simultaneous removal of the radiotoxic nuclides Cs137 and I129 from aqueous solution, Sep. Purif. Technol. 12 (1997) 215–227.
[24] J. Kim, J. Kang, W. Um, Simultaneous removal of cesium and iodate using prussian blue functionalized CoCr layered double hydroxide (PB-LDH), J. Environ. Chem. Eng. 10 (2022) 107477.
[25] D. Yang, S. Sarina, H. Zhu, H. Liu, Z. Zheng, M. Xie, S.V. Smith, S. Komarneni, Capture of radioactive cesium and iodide ions from water by using titanate nanofibers and nanotubes, Angew. Chem. Int. Ed. 50 (2011) 10594–10598.
[26] S.-E. Bae, D. Gokcen, P. Liu, P. Mohammadi, S.R. Brankovic, Size effects in monolayer catalysis—model study: Pt submonolayers on au (111), Electrocatalysis 3 (2012) 203–210.
[27] W. Chen, X.H. Xia, Highly stable nickel hexacyanoferrate nanotubes for electrically switched ion exchange, Adv. Funct. Mater. 17 (2007) 2943–2948.
[28] D. Choi, Y. Cho, S.-E. Bae, T.-H. Park, Study of electrochemical Cs uptake into a nickel hexacyanoferrate/graphene oxide composite film, J. Electrochem. Sci. Technol. 10 (2019) 123–130.
[29] S.J. Gerber, E. Erasmus, Electronic effects of metal hexacyanoferrates: an XPS and FTIR study, Mater. Chem. Phys. 203 (2018) 73–81.
[30] S.-J. Park, S.S. Shin, J.H. Jo, C.H. Jung, H. Park, Y.-I. Park, H.-J. Kim, J.-H. Lee, Tannic acid-assisted in-situ interfacial formation of Prussian blue-assembled adsorptive membranes for radioactive cesium removal, J. Hazard Mater. 442 (2023) 129967.
[31] X. Jin, L. Huang, S. Yu, M. Ye, J. Yuan, J. Shen, K. Fang, X. Weng, Selective electrochemical removal of cesium ion based on nickel hexacyanoferrate/reduced graphene oxide hybrids, Sep. Purif. Technol. 209 (2019) 65–72.
[32] A. Doménech, N. Montoya, F. Scholz, Estimation of individual Gibbs energies of cation transfer employing the insertion electrochemistry of solid Prussian blue, J. Electroanal. Chem. 657 (2011) 117–122.
[33] H.-W. Lee, M. Pasta, R.Y. Wang, R. Ruffo, Y. Cui, Effect of the alkali insertion ion on the electrochemical properties of nickel hexacyanoferrate electrodes, Faraday Discuss 176 (2014) 69–81.
[34] M.P. Soriaga, A.T. Hubbard, Determination of the orientation of aromatic molecules adsorbed on platinum electrodes: the influence of iodide, a surface-active anion, J. Am. Chem. Soc. 104 (1982) 2742–2747.
[35] J. Wang, X. Guo, Adsorption isotherm models: classification, physical meaning, application and solving method, Chemosphere 258 (2020) 127279.
[36] J. Wang, X. Guo, Adsorption kinetic models: physical meanings, applications, and solving methods, J. Hazard Mater. 390 (2020) 122156.
[37] X. Guo, J. Wang, Comparison of linearization methods for modeling the Langmuir adsorption isotherm, J. Mol. Liq. 296 (2019) 111850.
[38] M.A. Al-Ghouti, D.A. Da'ana, Guidelines for the use and interpretation of adsorption isotherm models: a review, J. Hazard Mater. 393 (2020) 122383.